






Intensive cycling of nickel in a New Caledonian forest dominated by hyperaccumulator trees

Adrian L. D. Paul¹ , Sandrine Isnard^{2,3} , Christine M. Wawryk⁴, Peter D. Erskine¹ , Guillaume Echevarria^{1,5} , Alan J. M. Baker^{1,5,6}, Jason K. Kirby⁴ and Antony van der Ent^{1,5,*} 

¹Centre for Mined Land Rehabilitation, Sustainable Minerals Institute, The University of Queensland, Brisbane, QLD 4072, Australia,

²AMAP, University of Montpellier, IRD, CIRAD, CNRS, INRAE, Montpellier 34980, France,

³AMAP, Herbar de Nouvelle-Calédonie, IRD, Nouméa 98848, Nouvelle Calédonie,

⁴Land and Water Business Unit, Industry Environments Program, Commonwealth Scientific and Industrial Research Organisation, Urrbrae, SA 5064, Australia,

⁵Laboratoire Sols et Environnement, Université de Lorraine-INRAE, Vandœuvre-lès-Nancy 54500, France, and

⁶School of BioSciences, The University of Melbourne, Parkville, VIC 3010, Australia

Received 3 March 2021; revised 11 May 2021; accepted 21 May 2021; published online 30 May 2021.

*For correspondence (e-mail a.vanderent@uq.edu.au).

SUMMARY

The hyperaccumulator *Pycnandra acuminata* is a New Caledonian rainforest tree known to have the highest concentration of nickel in any living organism, with 25 wt% nickel in its latex. All trees (with a diameter of >10 cm) and soil profiles in a 0.25-hectare permanent plot were sampled to assess the biogeochemical compartmentalisation of nickel in a dense stand of *P. acuminata* trees. Nickel stable isotope analysis permitted insights into the cycling of nickel in this ecosystem. The total tree biomass of the plot was calculated to be 281 tonnes ha⁻¹, which contained 0.44 kg of cobalt, 49.1 kg of manganese, 257 kg of nickel and 6.76 kg of zinc. Nickel stable isotope analysis identified the biotic origin of the nickel in the soil upper layers, with *P. acuminata* shoots enriched in lighter nickel isotopes. The $\delta^{60}\text{Ni}$ latex signature suggests that long-distance transport, radial xylem and phloem loading are at play in *P. acuminata*.

Keywords: biogeochemical cycle, nickel, *Pycnandra acuminata*, stable isotope, latex.

INTRODUCTION

Plants capable of attaining very high concentrations of trace elements in living shoots of at least 100–1000 times greater than most other plants are termed ‘hyperaccumulators’ (Reeves, 1992, 2003; van der Ent *et al.*, 2012). Throughout the world, approximately 700 species and 130 genera in 50 plant families are known to hyperaccumulate a range of trace elements (e.g. manganese, cobalt and zinc), with nickel (Ni) hyperaccumulators accounting for >70% of the known reports (Reeves *et al.*, 2021). Hyperaccumulator plants have been the subject of intensive research for almost half a century for their potential use in applications such as phytoremediation, phytoextraction and phytomining (Nkrumah *et al.*, 2016; Rascio and Navarri-izzo, 2011).

Hotspots for hyperaccumulator plants are mostly located in tropical regions (e.g. Borneo, Cuba, Brazil and New Caledonia) (Isnard *et al.*, 2016; Reeves *et al.*, 1999, 2007; van der Ent *et al.*, 2015). The most extreme examples of

hyperaccumulation include plants capable of hyperaccumulating >1 wt% dry weight (DW) Ni (Galey *et al.*, 2017; Reeves *et al.*, 2007; van der Ent *et al.*, 2015). For example, *Phyllanthus balgooyi* Petra Hoffm. & A.J.M. Baker (Phyllanthaceae) has been reported to accumulate up to 16.0 wt % DW Ni in phloem sap and *Blepharidium guatemalense* Standl. (Rubiaceae) leaves accumulate up to 4.3 wt% DW Ni (Mesjasz-Przybylowicz *et al.*, 2016; Navarrete Gutiérrez *et al.*, 2021). However, the highest recorded concentration of Ni occurs in the blue-green latex of *Pycnandra acuminata* (Pierre ex Baill.) Swenson & Munzinger (formerly *Sebertia acuminata*, Sapotaceae), an endemic tree from the New Caledonian ultramafic rainforest with approximately 26 wt% DW Ni (Jaffré *et al.*, 1976, 2018).

New Caledonia, an archipelago located in the South-West Pacific, has a highly distinctive flora comprising approximately 3300 species of which >74% are endemic (Morat *et al.*, 2012). This species richness and uniqueness is likely to have resulted from climate, orography, soil type

and biotic interactions since the Eocene (Grandcolas *et al.*, 2008; Jaffré, 1993; Pillon *et al.*, 2020). Currently, 99 strong Ni-hyperaccumulating taxa ($>5000 \mu\text{g g}^{-1}$ Ni in the foliar dry matter) have been identified from New Caledonia from X-ray fluorescence (XRF) scanning of herbarium specimens, mostly from the families Cunoniaceae, Phyllanthaceae and Salicaceae (Gei *et al.*, 2020). In New Caledonia, Ni-hyperaccumulator plants represent 3.8% of the dicotyledonous plant diversity, which is approximately 25-fold greater than the worldwide average: this is likely to be a consequence of the prolonged exposure to ultramafic soils (covering a third of the main island of New Caledonia), containing high concentrations of metals such as Ni (from 0.2 wt% Ni to more than 1.0 wt% Ni) (Gei *et al.*, 2020; Isnard *et al.*, 2016). The evolution of metal tolerance/hyperaccumulation in plants occurs locally from clades with physiological pre-adaptations (notably in the orders Oxalidales and Malpighiales), as plants are immobile and the selective forces of metal toxicities are unambiguous (Baker, 2009; Baker *et al.*, 2010; Gei *et al.*, 2020; Pillon *et al.*, 2010).

As a consequence of their value for the mining industry (source of Ni), the pedogenic processes leading to their formation, and their unique floras, ultramafic soils have been studied intensively (Brooks, 1987). The parent bedrock is the main factor influencing soil pedogenesis. However, the climate, topography and vegetation cover (on shallow soils) are also significant factors in soil pedogenesis (Alexander and DuShey, 2011; Echevarria, 2021). Ultramafic soils are characterised by a low calcium (Ca)/magnesium (Mg) quotient and by high concentrations of trace elements, including cobalt (Co), chromium (Cr), manganese (Mn) and Ni. In New Caledonia, the soils can be divided into two major types: (i) 'brown soils' (magnesian Cambisols), found over serpentinite (or highly serpentinized peridotite) in geological contact areas (ultramafic/non-ultramafic) and locally occur principally at the base of the ultramafic massifs on the West coast of Grande Terre; and (ii) 'lateritic soils' (Ferralsols), which are common on the ultramafic peridotite massifs (plateaux or low-slope areas) that often develop a hematite hardpan, locally known as 'cuiresse' (Latham *et al.*, 1978; Tercinier, 1963). Maquis (i.e. low sclerophyll evergreen scrublands) and humid rainforest are the two main vegetation types on the New Caledonian ultramafic soils (Isnard *et al.*, 2016). Maquis communities have a diverse flora adapted to repeated fire events and extreme edaphic conditions, including low nutrients, lack of organic matter content and the formation of hardpans (Jaffré, 1980). Rainforests develop on deeper soils, have higher nutrient status as a result of preserved humus layers and A1 horizons, and are hence less edaphically limited (Isnard *et al.*, 2016; McCoy *et al.*, 1999). Both maquis and rainforests on ultramafic soils have very high levels of endemism ($>95\%$) and have

approximately 840 and 670 obligate endemic species, respectively (Isnard *et al.*, 2016).

Previous research on New Caledonian ultramafic soils has primarily focused on the discovery of Ni hyperaccumulator species, or describing the endemic flora and the factors that have structured it over time (Gei *et al.*, 2020; Isnard *et al.*, 2016; Jaffré, 1980; Jaffré and L'Huillier, 2010; Pillon *et al.*, 2010, 2020). There has been little work undertaken in examining the biogeochemical cycling of trace elements, such as Ni, in ultramafic rainforest and its relationship to hyperaccumulator plants. Soils throughout the world typically contain up to 450 mg kg^{-1} Ni, but ultramafic soils may contain $>10\,000 \text{ mg kg}^{-1}$ Ni, with phytoavailable concentrations up to 700 mg kg^{-1} diethylenetriaminepentaacetic acid (DTPA)-extractable Ni (Datta *et al.*, 2015; Galey *et al.*, 2017; Lopez *et al.*, 2019; van der Ent *et al.*, 2012). Hyperaccumulator species, through highly enhanced Ni-uptake mechanisms, are thought to benefit from the accumulation of toxic Ni in their tissues as a defence against herbivores and pathogens (the so-called 'defensive enhancement hypothesis') (Boyd, 2007, 2012). In addition, hyperaccumulators might benefit from the accumulation of Ni through their leaf litter, which can potentially exert a selective pressure to reduce the fitness of competing plant and microbial species (e.g. reduction of their germination rates and growth rates) and favour the survival of the offspring of hyperaccumulator species (Boyd and Martens, 1998; Schlegel *et al.*, 1991; van der Ent *et al.*, 2015). Elemental allelopathy, through the phyto-enrichment of soil Ni from litterfall, has been reported for *P. acuminata* as the litter and surface soil under *P. acuminata* trees were found to be significantly enriched in Ni (Boyd and Jaffré, 2001). In contrast, the upper soil layer in the vicinity of *P. acuminata* trees was not significantly enriched in other trace elements (e.g. Co, Mn and Zn), suggesting that *P. acuminata* does not interfere, at least directly, with the cycling of these elements. However, several potentially strong Co hyperaccumulator species do occur in the studied area, including *Hybanthus austrocaledonicus* Melch. (Violaceae), *Kermadecia pronyensis* (Guillaumin) Guillaumin (Proteaceae) and *Spiraeanthemum meridionale* (Hoogland) Pillon (Cunoniaceae) and could, as with *P. acuminata* for Ni, lead to litter enrichment and hence play a role in Co cycling.

The use of multi-collector inductively coupled plasma mass spectrometry (MC-ICP-MS) is increasingly used to investigate the fate and pathways of non-traditional metals such as Ni in soil-plant systems through isotopic fractionation (Ratié *et al.*, 2019; Zelano *et al.*, 2018). The Ni isotopic composition of hyperaccumulator plants has been found to range from -1.0 to 1.3‰ $\delta^{60}\text{Ni}$ (Deng *et al.*, 2014; Ratié *et al.*, 2019). Several mechanisms can be involved in the uptake and translocation of Ni in hyperaccumulator plants that can lead to Ni fractionation (Zelano *et al.*, 2020),

including adsorption at root surfaces, uptake mechanisms and complexation with citrate ligands during translocation (Zelano *et al.*, 2018). Different findings for Ni fractionation have been reported for the same plant species at different phenological stages, indicating the complexity of the mechanisms involved during growth and development stages (Deng *et al.*, 2014; Estrade *et al.*, 2015). In *Rinorea* cf. *bengalensis* (Wall.) Kuntze. (Violaceae), differences between apical and basal leaves were observed for an individual of 1.5 m in height, with the $\Delta^{60}\text{Ni}_{\text{young_leaves} - \text{old_leaves}}$ value reaching -0.23‰ , but no trend was observed in plants of 6 m in height (Zelano *et al.*, 2020). This suggests that the translocation of lighter Ni isotopes from roots to young leaves is offset in older specimens, with young leaves becoming more enriched in heavier Ni isotopes through continuous phloem loading and unloading (Zelano *et al.*, 2020).

The present study aimed to determine the extent to which large Ni hyperaccumulator trees can alter the biogeochemical cycling of Ni and other trace elements in a tropical ultramafic ecosystem. To that end, we assessed all of the Co, Mn, Ni and Zn pools (in soil, plant tissues and debris/litter) in a model rainforest ecosystem dominated by *P. acuminata* in New Caledonia. The high-density stand of *P. acuminata* and the dominance of the Sapotaceae, which account for 15% of the trees in the plot [six species, including three sympatric *Pycnandra* spp.: *P. acuminata*, *Pycnandra fastuosa* (Baill.) Vink and *Pycnandra sessilifolia* (Pancher & Sebert) Swenson & Munzinger], made this plot particularly attractive for such an investigation. Two approaches were used, the first was based on the interpolation of soil and plant analytical data (Co, Mn, Ni and Zn) to evaluate the influence of *P. acuminata* on the ecosystem (e.g. modification of species distribution, phytoenrichment or depletion of the rhizosphere) and ultimately to compare biogeochemical cycling within the main trace elements; and the second used the stable Ni isotope ratios to examine the distribution and fate of Ni in this soil–plant system.

RESULTS

Nickel concentrations in hyperaccumulator plant species in the plot

The most abundant hyperaccumulator tree was *P. acuminata*, with a total of 22 individuals. The majority of these trees had a diameter of <20 cm (14 out of 22, with a median diameter of 16.6 cm), with the largest tree being approximately 25 m in height with a stem diameter of 47.1 cm. Its blue–green latex had the highest concentration of Ni collected at the site, with an average of $64\,500\text{ }\mu\text{g g}^{-1}$ and a maximum of $77\,000\text{ }\mu\text{g g}^{-1}$ Ni. The other plant parts were also enriched in Ni, but only the twigs exceeded $10\,000\text{ }\mu\text{g g}^{-1}$ Ni. Young leaves, old leaves, bark ($>6000\text{ }\mu\text{g g}^{-1}$) and wood ($2310\text{ }\mu\text{g g}^{-1}$) had lower, but

nonetheless very high Ni concentrations (Table 1). The second most common hyperaccumulator tree species in the plot was *Geissois pruinosa* Brongn. & Gris var. *pruinosa* (Cunoniaceae), with four individuals. The largest individual had a stem diameter of 29.3 cm. Nickel concentrations were highest in the leaves and twigs ($>3000\text{ }\mu\text{g g}^{-1}$) in this species, with up to $9830\text{ }\mu\text{g g}^{-1}$ in old leaves, and were lower in the bark, wood and xylem sap, with means of approximately $1000\text{ }\mu\text{g g}^{-1}$, $250\text{ }\mu\text{g g}^{-1}$ and 6.23 mg L^{-1} , respectively (Table 1). Two *Homalium guillauminii* Briq. (Salicaceae) trees were also growing in the plot (with stem diameters of 10.0 and 15.9 cm). This species had relatively low Ni concentrations, with only the leaves exceeding the hyperaccumulation threshold ($1000\text{ }\mu\text{g g}^{-1}$) and contained up to $1700\text{ }\mu\text{g g}^{-1}$ Ni. All the other plant parts had concentrations of $<500\text{ }\mu\text{g g}^{-1}$ and the xylem sap Ni concentrations were up to 12.9 mg L^{-1} (Table 1). Two additional hyperaccumulator shrub species, *Psychotria gabriellae* (Baill.) Guillaumin (Rubiaceae) and *H. austrocaledonicus*, with the former having the capacity to concomitantly hyperaccumulate Co and Ni, were present in the plot, but had stem diameters of <10 cm and therefore not sampled. Among the 60 non-hyperaccumulating tree species in the plot, three additional species, *Planchonella endlicheri* (Montrouz.) Guillaumin, *Pycnandra sessilifolia* and *Pleurocalyptus pancheri* (Brongn. & Gris) (J.W. Dawson), exceeded the Ni hyperaccumulation threshold, with at least one individual having $>1000\text{ }\mu\text{g g}^{-1}$ foliar Ni (Table 1). Overall, the median concentration of Ni in the non-hyperaccumulator trees was $<50\text{ }\mu\text{g g}^{-1}$, with the highest concentrations found in the twigs ($P < 0.001$). The main statistical parameter that influenced the concentration of Ni in the tissues of non-hyperaccumulators was the species ($P < 0.001$). In addition, the hyperaccumulator biomass index (HBI) was also statistically significant in determining Ni concentrations in all tissues, except for the bark, in the non-hyperaccumulators (Table S1). Other parameters, such as diameter at breast height (dbh), were not significant, whereas the species composition around hyperaccumulator trees could not be predicted.

Concentrations of the most common trace elements in trees from the plot

Cobalt and Zn concentrations were significantly higher in the Ni hyperaccumulating trees for each of the plant parts (Tables S2 and S3). For Co, the medians were at least twice as high in hyperaccumulator trees compared with non-hyperaccumulator trees (the ratios ranged from 2 in bark to 21 in young leaves), but none reached the Co hyperaccumulation threshold ($300\text{ }\mu\text{g g}^{-1}$), as the maximum concentration was $161\text{ }\mu\text{g g}^{-1}$ Co (in twigs of a *G. pruinosa* var. *pruinosa* tree). The Zn concentrations in plant parts were approximately four times greater in hyperaccumulator tree species, but the concentrations were low

Table 1 Nickel concentrations in diverse plant parts (young leaves, old leaves, twigs, bark, wood, latex and xylem sap) of the Ni-hyperaccumulator species and other major families present in the plot.

Family/Species	n	Young leaves	Old leaves	Twigs	Bark	Wood	Latex	Xylem sap
Hyperaccumulators	29	5770 (299–17 900)	3460 (252–16 000)	11 300 (182–20 200)	6700 (59.2–13 400)	1980 (53.3–4910)	–	5.27 (3.03–23.8)
<i>Pycnantha acuminata</i>	22	8650 (299–17 900)	6540 (252–16 000)	12 000 (3020–20 200)	7390 (1210–13 400)	2310 (1290–4910)	64 500 (57 100–76 600)	–
<i>Geissois pruinosa</i> var. <i>pruinosa</i>	4	3640 (2680–6830)	3780 (3140–9830)	3030 (1420–5310)	1070 (620–1670)	261 (182–472)	–	6.23 (3.03–23.8)
<i>Homalium guillauminii</i>	2	956 (385–1530)	1040 (370–1700)	265 (182–347)	109 (59.2–158)	67.7 (53.3–82.2)	–	8.59 (4.31–12.9)
Non-hyperaccumulators	173	27.4 (4.24–1510)	43.4 (6.34–1830)	48.3 (1.44–1890)	36.3 (4.49–615)	15.5 (0.18–302)	–	1.76 (0.10–14.2)
Sapotaceae ^a	29	346 (4.31–4900)	303 (7.11–4480)	302 (8.91–1890)	192 (4.49–615)	129 (0.18–302)	18.6 (0.92–45.5)	–
<i>Planchonella endlicheri</i>	16	37.4 (13.1–4900)	65.4 (32.5–4480)	132 (71.0–1890)	144 (79.5–615)	149 (54.9–302)	6.37 (1.27–11.9)	–
Myrtaceae	24	21.4 (5.21–1320)	38.0 (14.2–1400)	38.0 (9.78–424)	36.3 (8.33–366)	14.3 (4.40–187)	–	2.00 (0.55–14.2)
<i>Pleurocalyptus pancheri</i>	10	22.2 (11.3–1320)	27.3 (14.2–1400)	33.0 (17.3–424)	37.9 (15.1–3656)	11.4 (5.00–187)	–	4.72 (1.24–14.2)
Sapindaceae ^b	10	57.6 (17.7–80.2)	65.0 (25.6–136)	57.2 (20.9–168)	148 (71.6–206)	25.4 (4.18–76.7)	–	2.15 (1.21–2.49)
<i>Storthocalyx chryseus</i>	21	46.5 (16.0–91.8)	33.9 (8.99–241)	78.0 (22.0–391)	32.4 (14.6–265)	10.0 (1.70–64.8)	–	1.34 (0.55–13.3)
Bignoniaceae ^b	9	59.0 (47.0–148)	92.4 (38.3–229)	141 (84.5–268)	99.0 (45.1–214)	40.4 (7.80–71.3)	–	1.97 (0.22–4.78)
<i>Deplanchea speciosa</i>								
Moraceae ^b								
<i>Sparattosyce dioica</i>								

Concentrations ($\mu\text{g g}^{-1}$) are summarised as median (min.–max.).^aOnly the non-hyperaccumulator species of the family was considered.^bFamily with only one species.

(maximum was $168 \mu\text{g g}^{-1}$). In contrast to Co and Zn, Mn concentrations tended to be lower in Ni hyperaccumulator tree species, but significant statistical differences were only found for the old leaves (Table S4). No significant statistical differences between hyperaccumulator and non-hyperaccumulator trees were observed for Al or Cr, elements that are indicators of potential soil particulate contamination. Species was the main and only significant parameter for Mn and Zn concentrations in non-hyperaccumulator tree species ($P < 0.001$). In contrast, weak, but significant, correlations were found between HBI and Co concentrations in all plant parts except for the bark of non-hyperaccumulator trees ($P \approx 0.03$).

Soil chemistry of the plot

A shallow eroded Ferralsol underlies the 0.25-ha plot (average gradient of the slope approx. 26%) and includes a topographic feature: a gully located on the western part,

which extends across the plot. The pH varied from approximately 4.0 to 6.5 in the plot, but did not change across the soil profile (0–20 cm depth; Table S5). The distribution of concentrations of exchangeable soil Ni [$\text{Sr}(\text{NO}_3)_2$ - and Ni DTPA-extractable] are heterogeneous in the plot (Figures 1 and 2; Table 2). The lowest exchangeable $\text{Sr}(\text{NO}_3)_2$ Ni concentrations were found in the eastern part of the plot (approx. 5.00 mg kg^{-1}) and a notable 'hotspot' area was found in the north-west area (approx. 21.0 mg kg^{-1}), which corresponded to the area with the lowest exchangeable Mn concentrations (approx. 30 mg kg^{-1} in the topsoil). Total Ni was also significantly higher in the western half of the plot, with concentrations up to 1200 mg kg^{-1} in the north-west area (Figure 3). In contrast, Co had higher phytoavailable concentrations in the centre of the plot (north, centre and south areas), with concentrations $>60 \text{ mg kg}^{-1}$. Cobalt, Mn and Zn all had higher exchangeable concentrations in the southern section of the plot with, respectively,

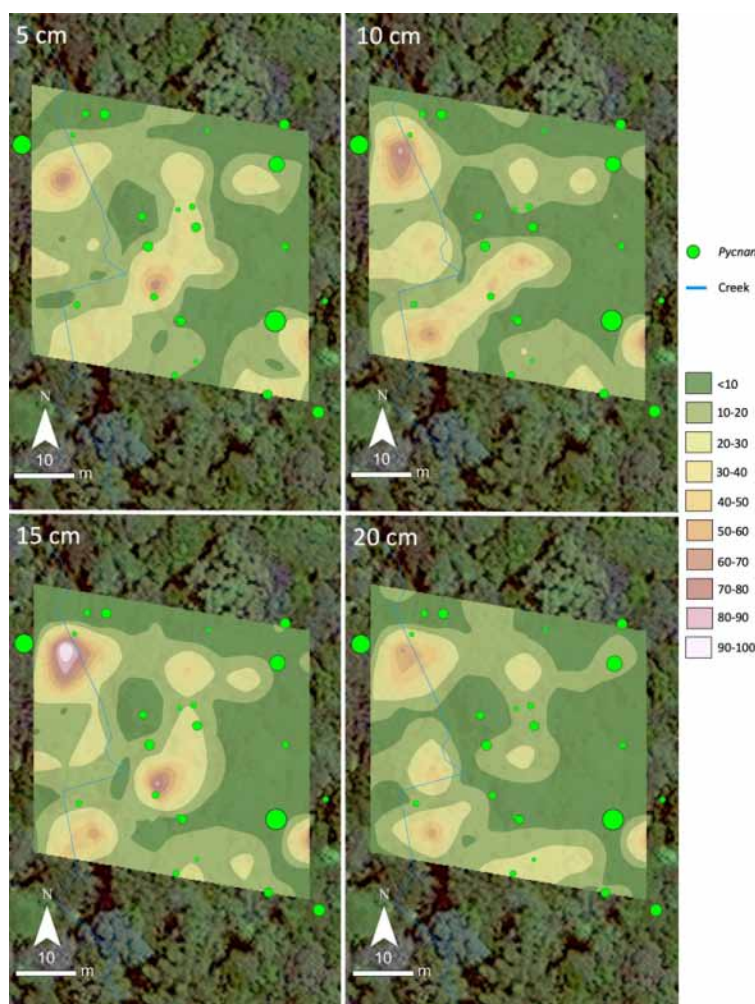


Figure 1. Spatial distribution of $\text{Sr}(\text{NO}_3)_2$ -extractable Ni concentrations (mg kg^{-1}) at four different depths (5, 10, 15 and 20 cm) across the tropical forest plot in the Plaine des Lacs, New Caledonia. Each map is based on 100 (one per subplot) 20-cm-deep soil cores.

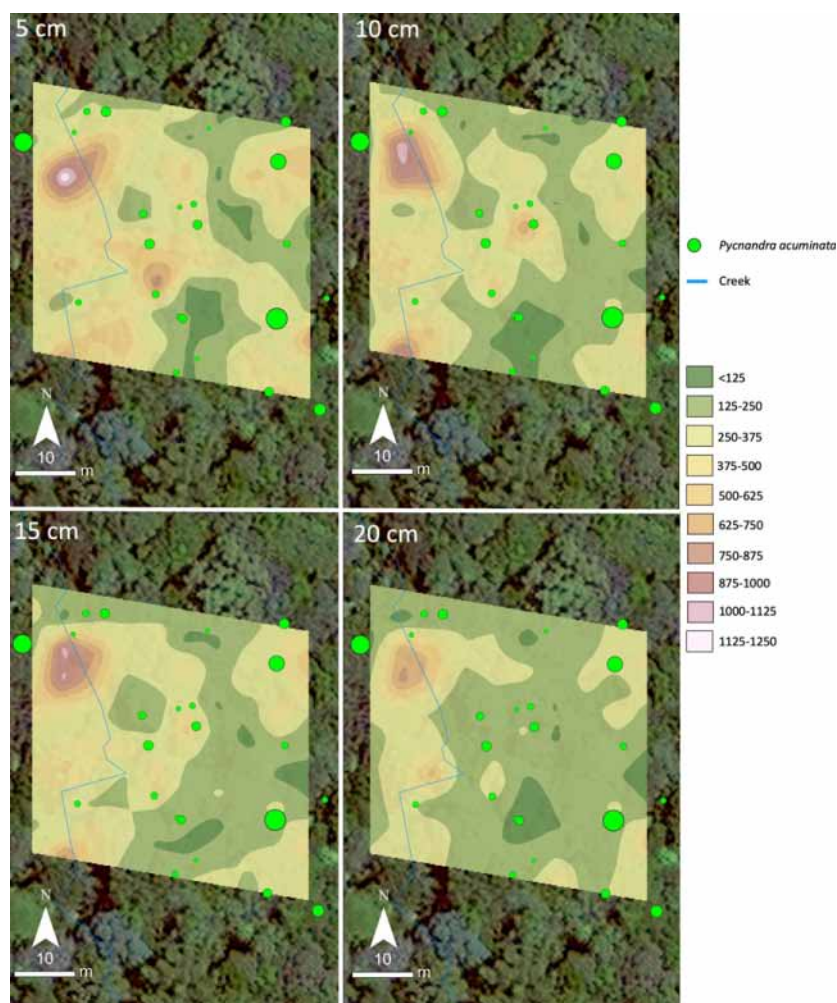


Figure 2. Spatial distribution of diethylenetriaminepentaacetate (DTPA)-extractable Ni concentrations (mg kg^{-1}) at four different depths (5, 10, 15 and 20 cm) across the tropical forest plot in the Plaine des Lacs, New Caledonia. Each map is based on 100 (one per subplot) 20-cm-deep soil cores.

Table 2 Soil profile chemistry in the plot (one sample per subplot: 100 samples)

	Depth (cm)	Co	Mn	Ni	Zn
Total	0–5	414 (70.6–674)	2790 (365–6650)	4100 (837–6500)	162 (66.4–253)
	5–10	562 (275–788)	3600 (1700–6630)	5060 (2420–7980)	190 (98.2–251)
	10–15	589 (215–791)	3760 (1190–6750)	5210 (2280–7470)	202 (145–245)
	15–20	615 (323–868)	4070 (1850–7980)	5400 (3120–9700)	208 (133–338)
DTPA-extractable	0–5	58.8 (14.5–159)	374 (36.1–830)	335 (93.7–1180)	11.9 (5.42–28.8)
	5–10	57.3 (14.0–135)	407 (90.0–612)	275 (65.2–1080)	6.76 (2.62–24.7)
	10–15	61.0 (15.5–119)	411 (71.7–696)	273 (73.2–1000)	8.29 (3.24–27.2)
	15–20	47.3 (8.47–104)	380 (115–650)	216 (50.3–787)	5.40 (2.68–24.5)
$\text{Sr}(\text{NO}_3)_2$ -extractable	0–5	2.67 (0.12–10.2)	40.9 (<LoD–146)	12.5 (0.97–69.7)	0.48 (0.06–3.50)
	5–10	1.66 (0.05–16.8)	19.9 (<LoD–181)	12.2 (1.49–79.7)	0.25 (0.02–1.58)
	10–15	1.96 (0.02–17.8)	25.8 (<LoD–265)	12.3 (1.51–103)	0.32 (0.02–5.39)
	15–20	1.06 (0.01–10.8)	0.27 (<LoD–116)	10.6 (1.26–60.4)	0.23 (0.02–2.33)

Concentrations (mg kg^{-1}) are summarised as median (min–max). LoD, limit of detection.

>6.00, >20.0 and >0.70 mg kg⁻¹ down the soil profile (Figures S1–S9; Table 2). Although differences were found between sub-areas for phytoavailable Mn and Zn concentrations, no clear geographical pattern was distinguishable.

Overall, the concentrations of exchangeable soil Ni were higher in the top 15 cm, whereas the opposite was found for total Ni, which was higher in the deeper soil. Exchangeable Co, Mn and Zn showed similar patterns to Ni, with lower concentrations in the deeper soil horizons (Figures S10–S17; Table 2). Except for Mn, the average phytoavailable concentrations of trace elements varied according to depth, with lower concentrations in the deepest layer and higher concentrations in the surface soil (approx. 45 versus 60 mg kg⁻¹ for Co, approx. 240 versus 350 mg kg⁻¹ for Ni and approx. 6 versus 12 mg kg⁻¹ for Zn). However, location was the main parameter influencing soil phytoavailable concentrations.

Total concentrations of trace elements varied significantly down the depth gradient, with higher Co, Mn, Ni and Zn concentrations in the deepest soil layer (Figures 3, S3, S6 and S9; Table 2). Concurrently, weaker, but significant, locational differences were detected (other than for Mn). The average total concentrations of Al, Co and Cr varied down the soil profile, approximately 2000–18 000, 70.6–870 and 1000–6000 mg kg⁻¹, respectively, but no clear pattern emerged. 'Hotspot' areas were observed for Mn and Zn in the deepest soil layers, as Mn was enriched in the eastern area (>3500 mg kg⁻¹ down the soil profile) and Zn was slightly enriched in the north-west and south-east areas of the plot (approx. 200 mg kg⁻¹). The total Ni concentrations were relatively higher in the western part of the plot, with concentrations up to approximately 8200 mg kg⁻¹. Cobalt concentrations varied considerably according to location and sample depth. However, no

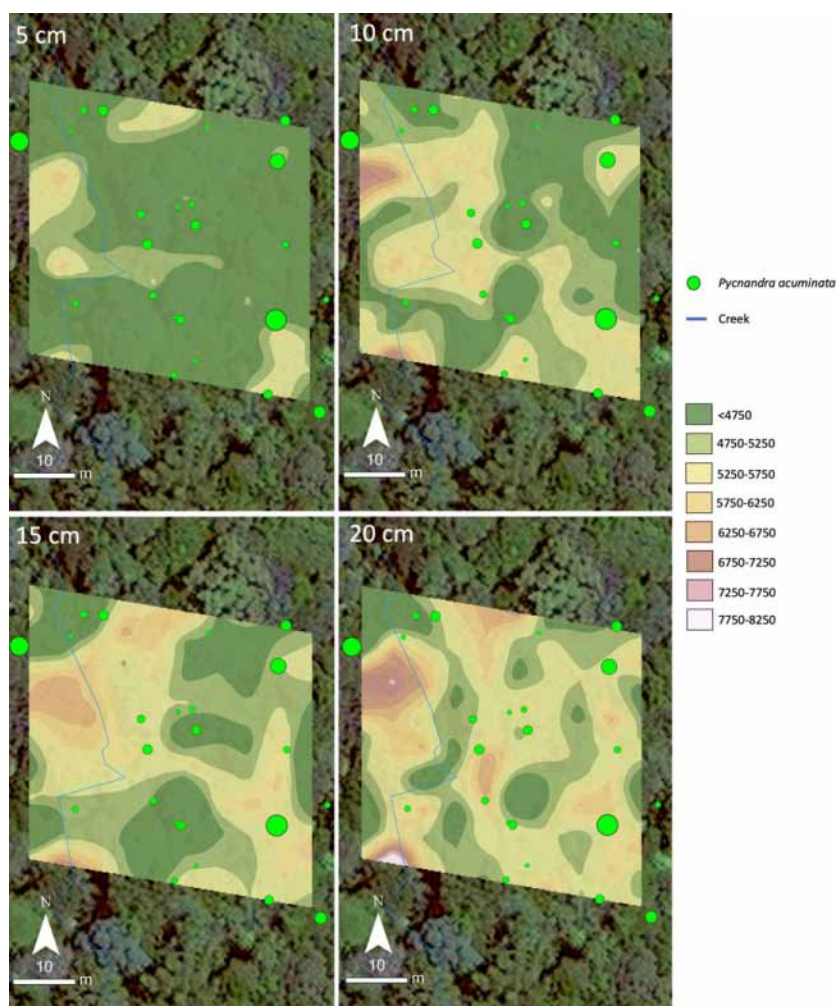


Figure 3. Spatial distribution of total Ni concentrations (mg kg⁻¹) at four different depths (5, 10, 15 and 20 cm) across the tropical forest plot in the Plaine des Lacs, New Caledonia. Each map is based on 100 (one per subplot) 20-cm-deep soil cores.

clear distribution pattern could be observed. Totals of approximately 350, 2500, 3200 and 125 kg of Co, Mn, Ni and Zn, respectively, in the first 20 cm of the plot were calculated.

Statistical analyses revealed that all pools of Ni were negatively correlated with the HBI ($P < 0.001$), whereas depth was positively correlated with the total Ni values and was negatively correlated with the extractable Ni values ($P < 0.001$). In contrast, positive correlations were found for Co and HBI for total Co concentrations ($P < 0.001$) and weakly exchangeable Co concentrations ($P < 0.005$). Available Zn concentrations (weakly exchangeable and potentially phytoavailable) were positively correlated with HBI, whereas total concentrations were negatively correlated ($P < 0.001$). No pattern could be observed for Mn, however, depth was negatively correlated ($P < 0.001$) with Mn available pools and positively correlated ($P < 0.001$) with total concentrations. In the topsoil, the pH was correlated with total Co ($P = 0.006$), Ni and Zn ($P < 0.001$), and potentially phytoavailable Ni ($P < 0.001$). No significant correlation was found in the deeper layers, except at 15 cm for available Ni concentrations ($P < 0.001$).

Quantities of trace elements in living standing tree biomass

Calculated total quantities of trace elements in the standing biomass of the trees in the plot are given in Table 3. In this study, trees were divided into three parts: stems, branches and leaves. It was calculated that stems (including the trunk) represented approximately 85%, branches approximately 14%, and leaves approximately 1% of the

tree biomass. The total biomass of the plot (dbh > 10 cm), including hyperaccumulators and non-hyperaccumulators, was calculated to be 281 tonnes ha^{-1} . Based on these calculations, there is 0.44 kg ha^{-1} of Co, 49.1 kg ha^{-1} of Mn, 257 kg ha^{-1} of Ni and 6.76 kg ha^{-1} of Zn contained in the standing tree biomass of the plot. Manganese and Zn were mostly contained in non-hyperaccumulator trees, with 92.3 and 66.2%, respectively, of the total quantities. However, a significant portion of Co (60.1%) and almost all the Ni (93.9%) was contained in the hyperaccumulator tree biomass (90.3% of which was in *P. acuminata*), despite the species representing <15% of the trees.

Leaf litterfall and trace element chemistry

The litterfall mass and quantities of trace elements returned to the soil over 12 months (from February 2018 to February 2019) are summarised in Tables 4 and S6. Weak but significant differences in litterfall mass were observed between litter traps (a trap had lower litterfall, $P = 0.004$). Significant differences were also found between the months of collection, as the weight of litterfall collected followed a seasonal pattern. The highest masses were collected during the October–February period and the lowest masses were collected during the April–August period, following the climatic trends, as low litterfall periods corresponded with periods of low precipitation and light wind regimes. Overall, quantities of all elements (Co, Mn, Ni and Zn) returned to soil followed the same trends, with higher quantities found between October and February (all maximum means were obtained for the November/December collection). From February 2018 to January 2019, this equated to a return of 16.5 g $\text{ha}^{-1} \text{ year}^{-1}$ of Co (with a maximum of

Table 3 Total mass of Co, Mn, Ni and Zn in trees (diameter at breast height, dbh > 10 cm for hyperaccumulator and dbh > 15 cm for non-hyperaccumulator trees) growing in the subplots and their relative quantities (%), based on the allometric formulae proposed by Yamakura *et al.* (1986) and Chave *et al.* (2014)

Family/Species	n	Co (g ha^{-1})	Mn (kg ha^{-1})	Ni (kg ha^{-1})	Zn (kg ha^{-1})
Hyperaccumulators	29	265 (60.1%)	3.77 (7.7%)	242 (93.9%)	2.28 (33.8%)
<i>Pycnantha acuminata</i>	22	73.1 (16.5%)	2.43 (4.9%)	232 (90.3%)	2.03 (30.0%)
<i>Geissois pruinosa</i> var. <i>pruinosa</i>	4	190 (43.0%)	1.16 (2.4%)	9.12 (3.5%)	0.15 (2.2%)
<i>Homalium guillainii</i>	2	2.42 (0.5%)	0.18 (0.4%)	0.25 (0.1%)	0.11 (1.6%)
Non-hyperaccumulators	173	176 (39.9%)	45.4 (92.3%)	15.7 (6.1%)	4.48 (66.2%)
Sapotaceae ^a	29 ^a	61.4 (13.9%)	8.79 (17.9%)	6.21 (2.4%)	0.99 (14.7%)
<i>Planchonella endlicheri</i>	16	45.9 (10.4%)	3.06 (6.2%)	4.48 (1.7%)	0.55 (8.1%)
Myrtaceae	24	18.6 (4.2%)	5.47 (11.1%)	2.42 (0.9%)	0.48 (7.0%)
<i>Pleurocalyptus pancheri</i>	10	10.1 (2.3%)	0.96 (2.0%)	1.55 (0.6%)	0.24 (3.5%)
Sapindaceae ^b	10	0.63 (0.1%)	0.94 (1.9%)	1.21 (0.5%)	0.34 (5.1%)
<i>Storthocalyx chryseus</i>					
Bignoniaceae ^b	21	8.74 (2.0%)	2.91 (5.9%)	1.61 (0.6%)	0.53 (7.9%)
<i>Deplanchea speciosa</i>					
Moraceae ^b	9	3.06 (0.7%)	1.04 (2.1%)	0.89 (0.3%)	0.16 (2.4%)
<i>Sparattosyce dioica</i>					
Total	202	442	49.1	257	6.76

^aQuantities of trace elements in non-hyperaccumulator Sapotaceae species.

^bFamily with only one species.

Table 4 Total quantities of trace elements returning to the soil via litterfall per month over 1 year

Month	Biomass (kg ha ⁻¹)	Co (g ha ⁻¹)	Mn (g ha ⁻¹)	Ni (g ha ⁻¹)	Zn (g ha ⁻¹)
Feb 18	1720 a (714–4880)	1.68 ab (0.44–4.44)	450 ab (77.7–1780)	398 b (24.1–1740)	23.0 ab (7.26–75.8)
Mar 18	435 abc (0–806)	0.66 cde (0.10–2.35)	189 abc (53.2–592)	82.5 cd (5.31–313)	6.99 cde (3.19–12.8)
Apr 18	238 c (130–419)	0.32 de (0.02–1.14)	104 c (29.2–392)	17.0 de (3.79–67.8)	3.93 ef (1.32–8.16)
May 18	395 c (0–1080)	0.36 cde (0–0.76)	155 c (0–674)	22.3 cde (0–58.4)	5.21 de (0–10.8)
Jun 18	93.0 d (0–241)	0.12 e (0–0.66)	62.7 d (0–237)	56.0 e (0–276)	2.65 f (0–14.2)
Jul/Aug 18 ^a	398 c (0–1300)	3.59 bcd (0–31.4)	162 c (0–527)	276 cd (0–2360)	18.9 cde (0–58.5)
Sept 18	533 bc (0–1230)	1.10 bc (0–2.08)	164 bc (0–301)	300 c (0–1500)	18.1 bc (0–33.2)
Oct 18	916 abc (0–1480)	2.41 a (0–6.58)	301 abc (0–921)	1110 ab (0–4350)	33.9 ab (0–76.9)
Nov/Dec 18 ^a	2250 ab (924–8060)	5.87 a (1.03–26.0)	994 a (288–2940)	2570 a (1060–9220)	83.3 a (29.3–277)
Jan/Feb 19 ^a	830 (0–2720) bc	2.08 (0–7.09) bcd	292 (0–978) c	203 (0–765) cd	20.9 (0–39.6) ab
Year (Total)	6090	16.5	2420	4640	194

Monthly means followed by the same letter are not significantly different at the 5% level according to the Waller–Duncan means separation test.

^aValues are for 2 months. Quantities (kg ha⁻¹ or g ha⁻¹) are summarised as median (min–max).

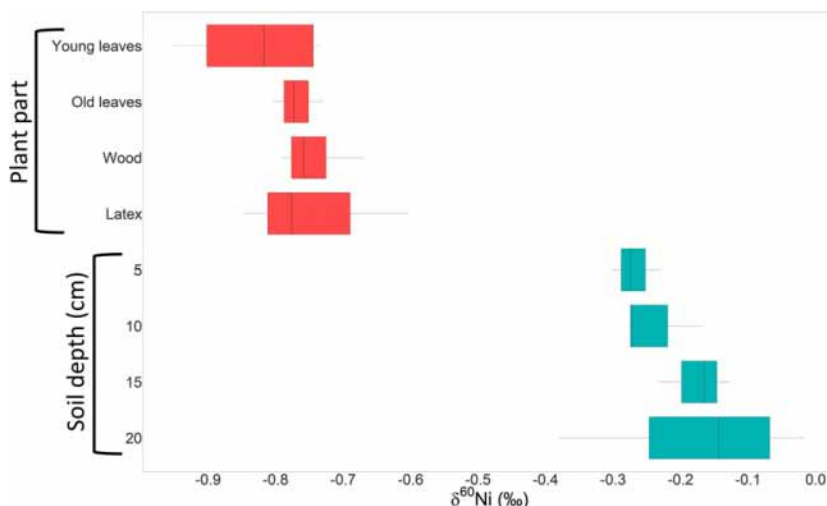


Figure 4. Nickel isotopic composition ($\delta^{60}\text{Ni}$ in ‰) of *Pycnanthus acuminatus* plant parts (red) and soil samples (blue) at four different depths (5, 10, 15 and 20 cm) collected in the same subplot.

5.87 g ha⁻¹ month⁻¹, 2420 g ha⁻¹ year⁻¹ of Mn (with a maximum of 994 g ha⁻¹ month⁻¹), 4640 g ha⁻¹ year⁻¹ of Ni (with a maximum of 2570 g ha⁻¹ month⁻¹), and 194 g ha⁻¹ year⁻¹ of Zn (with a maximum of 83.3 g ha⁻¹ month⁻¹).

Nickel stable isotopic composition of plant and soil samples

The shallow soil layers were slightly enriched in lighter Ni isotopes ($\delta^{60}\text{Ni}_{5\text{cm}} -0.27 \pm 0.04\text{‰}$, $\delta^{60}\text{Ni}_{10\text{cm}} -0.24 \pm 0.06\text{‰}$, $\delta^{60}\text{Ni}_{15\text{cm}} -0.18 \pm 0.05\text{‰}$ and $\delta^{60}\text{Ni}_{20\text{cm}} -0.20 \pm 0.18\text{‰}$ —Figure 4). In *P. acuminatus* tissues, $\delta^{60}\text{Ni}$ ratios are enriched in light Ni isotopes compared with soil samples (mean $\Delta^{60}\text{Ni}$ mean plant tissues – mean soil = -0.56‰ ; Figure 4). Similarly, young leaves of *P. acuminatus* were visibly enriched in

lighter Ni ($\delta^{60}\text{Ni} -0.86 \pm 0.10\text{‰}$) isotopes compared with older leaves ($\delta^{60}\text{Ni} -0.77 \pm 0.04\text{‰}$). No differences were observed in $\delta^{60}\text{Ni}$ ratios between old leaves, wood and latex.

DISCUSSION

In this study, the density of *P. acuminatus* trees (in a radius of >15 m) was negatively correlated with all Ni soil pools (exchangeable, phytoavailable and total), whereas for the entire plot, Ni concentrations in the trees were not correlated with Ni concentrations in the soils. However, extractable Ni was depleted in areas with greater HBIs, resulting from the uptake of Ni over hundreds of years by *P. acuminatus* trees capable of storing significant amounts of Ni in the living standing biomass. It is calculated that 232 kg of Ni was present in the biomass of *P. acuminatus* trees in the

plot, which represents 90.3% of all plant Ni and approximately 2.0% of all Ni (litterfall, living biomass and soil within the 0–20 cm horizon). Statistical analysis of HBI data did not reveal any species distributional differences between low- and high-density *P. acuminata* areas. In conjunction with a negative correlation with soil Ni, this fact suggests that Ni phytoenrichment is not important at the ecosystem scale. This process is attenuated by the large quantities of Ni that are returned to the topsoil around *Pycnandra* trees through litterfall, but the reuptake of Ni into *Pycnandra* trees appears to limit the accumulation of Ni in the surface soil. In rainforest systems, trees typically have shallow roots to capture as much of the nutrients (notably K and P) from litterfall as possible (Kerfoot, 1963), resulting in extremely tight biogeochemical cycles (Vitousek and Sanford, 1986). Although Ni is not limiting to plant growth in this plot, we propose that this similarly applies to Ni in the case of *P. acuminata* at this site, suggesting a possible side effect of the efficient recycling of K and P (which is yet to be determined). This hypothesis is supported by the statistically significant positive correlation found between the HBI and Ni concentrations in non-hyperaccumulator trees, suggesting that once it is available, Ni in *P. acuminata* litterfall is also taken up by non-hyperaccumulator trees. Our study was made at the plot scale and focused on the impact of an Ni-hyperaccumulator species in this ecosystem. Hence, it does not necessarily conflict with results previously obtained by Boyd and Jaffré (2001), suggesting an allelopathic effect of *P. acuminata* (with a fivefold enrichment of Ni under the canopy of *P. acuminata*) in the nearby Parc de la Rivière Bleue. The topography of the plot had a major effect on soil Ni distribution, as the accumulation of Ni in the gully may result from the leaching of Ni from Ni-rich material originating from further upstream (e.g. litterfall, leachate and eroded soil particles), which is subsequently captured in the colluvium, rich in clay minerals, at the base of the hill.

Despite the absence of large hyperaccumulator species of elements other than Ni, Co and Zn soil distribution had distinct patterns, further highlighting the key role of litterfall in this ecosystem. In areas with a higher density of *P. acuminata*, the available soil pools of Co were significantly higher. This correlation results from the higher Co uptake by Ni hyperaccumulator trees present in the plot, which contained >60% of all the 'biotic' Co. This leads to litterfall with significantly higher Co concentrations (calculated at $16.5 \text{ g ha}^{-1} \text{ year}^{-1}$) and eventually, after a long period, to a local enrichment, especially in available Co. A similar pattern was observed for Zn as a significant proportion of Zn present in the litterfall (calculated at $194 \text{ g ha}^{-1} \text{ year}^{-1}$) originates from the hyperaccumulator trees because of their higher Zn concentrations (>30% of biotic Zn and approximately fivefold more in old leaves). Hence, out of all of the trees in the plot, the Ni

hyperaccumulators had greater concentrations of Co and Zn (especially the Sapotaceae), likely resulting from similarities in uptake and translocation pathways of these elements and Ni (Deng *et al.*, 2016). Nonetheless, Co and Zn concentrations were relatively low compared with their respective hyperaccumulation thresholds ($300 \mu\text{g g}^{-1}$ for Co and $3000 \mu\text{g g}^{-1}$ for Zn). *Hybanthus austrocaledonicus*, one of the tree species in the plot (albeit none had a dbh of >10 cm), can accumulate concentrations up to $1000 \mu\text{g g}^{-1}$ Co and $58\,000 \mu\text{g g}^{-1}$ Ni, making it a Co and Ni hyperaccumulator (Paul *et al.*, 2020). Conversely, concentrations of Mn were lower in the Ni hyperaccumulator species, suggesting that they do not possess an efficient Mn transport system. Similar results have been reported in other hyperaccumulator plants (in the genera *Odontarrhena* and *Noccaea*, Brassicaceae), indicating that this phenomenon might be shared by most Ni hyperaccumulator species (Deng *et al.*, 2016; Ghaderian *et al.*, 2015).

Pycnandra acuminata tissues had significantly lower $\delta^{60}\text{Ni}$ values compared to the soil, which, as in another well-known tropical hyperaccumulator plant species, *Rinorea* cf. *bengalensis*, suggests that it preferentially takes up and/or translocates lighter Ni isotopes to its shoots (Zelano *et al.*, 2020). This finding contrasts with other studies reporting whole-plant or root isotopic compositions to be isotopically heavier compared with the soil for Ni hyperaccumulator species (Estrade *et al.*, 2015; Ratié *et al.*, 2019). It has been suggested that plant isotopic composition is mainly controlled by the root uptake process (Estrade *et al.*, 2015), although the processes leading to Ni fractionation in hyperaccumulator plants are not yet fully understood. However, it has been suggested that the uptake mechanisms occurring at the root cell membrane of hyperaccumulator plants may play an essential role in isotopic composition, as low-affinity transport across roots favours light isotope enrichment and high-affinity transport favours heavier isotopes (Deng *et al.*, 2014; Zelano *et al.*, 2018). Other mechanisms, such as the effect of Ni complexation with organic ligands in the rhizosphere, were determined to be marginal in causing an isotope fractionation of approximately -0.20‰ in the case of citrate (Zelano *et al.*, 2018). In soils that are not fully weathered (e.g. Cambisols), the available fraction (e.g. the DTPA-extractable fraction) may be enriched in heavy Ni isotopes through reactions/partitioning with solid phases in soils (Estrade *et al.*, 2015; Zelano *et al.*, 2020). The soil at Plaine des Lacs (i.e. Ferralsol) is relatively depleted in heavier isotopes ($\delta^{60}\text{Ni} = -0.21 \pm 0.04\text{‰}$), which may be a result of the continuous leaching of heavier Ni in pore water to deeper soil levels for extended time periods (Ratié *et al.*, 2015; Zelano *et al.*, 2020). Therefore, our results are fully consistent with those obtained for *R. cf. bengalensis* growing on a Ferralsol (SR₁₅₀) in Malaysia (Zelano *et al.*, 2020). Finally, it has also been shown that an enrichment of heavy Ni isotopes

down the soil profile is typical of rainforests with hyperaccumulator trees, the biomass of which is naturally enriched in lighter isotopes. This is because litterfall is likely to supply large quantities of light and available Ni isotopes to the topsoil, as with soil SR₁₅₀ in the Malaysian study (Zelano *et al.*, 2020).

In *P. acuminata*, wood and old leaves were slightly enriched in the heavier isotope, compared with young leaves ($\Delta^{60}\text{Ni}_{\text{old_leaves-young_leaves}} \approx 0.09\text{‰}$) and wood ($\Delta^{60}\text{Ni}_{\text{wood-young_leaves}} \approx 0.14\text{‰}$). This difference can be explained by the additional 'discriminatory' steps required for Ni to reach apical leaves, which involves complexation with organic ligands during transport. This would lead to preferential enrichment in heavier Ni isotopes and the preferential migration of lighter isotopes from wood to old and further young leaves, as part of the source-sink process and kinetic effects (with lighter isotopes moving faster). Isotopic fractionation of Ni between plant tissues has also been observed in other hyperaccumulator species, such as *Odontarrhena chalcidica* (Waldst. & Kit.) Endl. and *Noccaea caerulescens* (J. Presl & C. Presl) F.K. Mey., grown in hydroponic solutions, and young *R. cf. bengalensis* trees sampled in their native ultramafic environment (Deng *et al.*, 2016; Estrade *et al.*, 2015; Ratié *et al.*, 2019; Zelano *et al.*, 2020).

Our study is the first to demonstrate Ni isotope fractionation for a slow-growing large tree species, compared to species such as *R. cf. bengalensis* and *O. chalcidica*, which are much faster-growing species. Analyses using ¹⁴C have shown that *P. acuminata* tree boles in the same plot grow at approximately 1.5 mm year⁻¹, suggesting that the larger individuals may be five centuries or more old. In most studies, the plants were harvested for analysis at the flowering stage when phloem redistribution is at its highest (Estrade *et al.*, 2015; Zelano *et al.*, 2020). The underlying mechanisms responsible for Ni fractionation in *P. acuminata* are yet to be established, especially with regards to the role of the Ni-rich laticifer network in this species (Isnard *et al.*, 2020). Recent studies have revealed the crucial role of laticifers in Ni transport, which forms an independent and united system, in parallel with the traditional metal-transport paradigm that involves xylem loading, long-distance transport and translocation to leaves via the phloem (Isnard *et al.*, 2020). In *P. acuminata*, it is assumed that two non-mutually exclusive mechanisms occur concurrently, and their relative importance is unknown at present. The first mechanism involves the independent transport of Ni in laticifers throughout the plant from the roots (with Ni being directly loaded into laticifer ducts) using transient ligands and osmotic pressure, and would likely be less discriminatory than radial transport (favouring lighter isotopes). The second mechanism involves the passage of Ni from the xylem to laticifers via the phloem and is likely to lead to a heavier isotope enrichment.

The biogeochemical cycles of trace elements involve many abiotic and biotic processes that may be assessed via sophisticated sampling regimes and the use of advanced analytical methods, including stable isotope techniques. This study focused on a 0.25-ha plot that harbours the world's largest and most extreme Ni hyperaccumulator species, which has been shown to have a major influence on Ni cycling in this plot. This study did not reveal Ni phytoenrichment as a result of *P. acuminata* litterfall, and hence 'elemental allelopathy' does not appear likely to be important in this case. Further studies should focus on a mechanistic understanding of Ni fluxes in this system by measuring growth rates and Ni uptake by the *P. acuminata* trees in real time, in combination with measurements of stem flow and litter degradation.

EXPERIMENTAL PROCEDURES

Site location and description

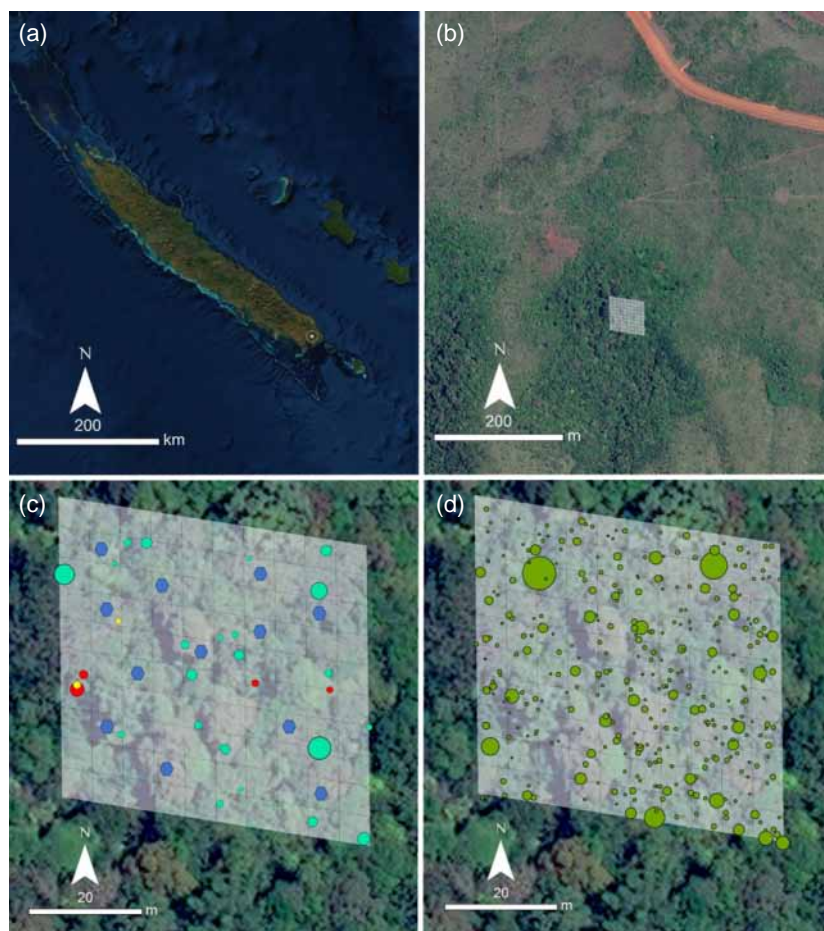
The study area was located in the southern part of Grande Terre, New Caledonia, in the Plaine des Lacs, south of 'Lac en Huit' (22°16'29"S, 166°54'14"E, approx. 270–300 m a.s.l.; Figure 5). Plot data were obtained from a 1-ha permanent rainforest area from the New Caledonian Plant Inventories and Permanent Plot Network (NC-PIPPN) inventory (<http://www.givd.info/ID/AU-NC-001>) (Birnbaum *et al.*, 2015; Ibanez *et al.*, 2013). All trees with a dbh of >10 cm were tagged and inventoried together with their relative position, dbh and height. Most of the species were identified on site, and specimens were also collected and compared with vouchers at the Herbarium of New Caledonia (NOU). Plant names followed FLORICAL nomenclature (Morat *et al.*, 2012; Munzinger *et al.*, 2021; continuously updated). This study used a 2500-m² portion of the larger 1-ha plot which contained 22 mature *P. acuminata* trees. The studied area was divided into 100 subplots, each of 25 m², for geospatial analysis and was then divided into nine subplots based on cardinal directions for descriptive purposes (NW, W, SW, etc.). The climate in the south of New Caledonia is subtropical and classified into two dominant seasons: a so-called 'hot season' from November to April, during which time both the precipitation and the temperatures are high (approx. 300 mm month⁻¹ and with a daily maximum temperature of 27–29°C), but moderated by trade winds and the maritime influence, and a 'cool season' from June to September, which is drier (150–250 mm month⁻¹) and cooler (Météo France, 2021).

Collection and processing of plant samples

Plant samples (old leaves, young leaves, twigs, bark, wood, xylem sap and latex) from hyperaccumulator species with a dbh of >10 cm or a dbh of >15 cm for the non-hyperaccumulator species were collected from March to May 2018 for subsequent chemical analysis (Figure 6). One branch (approx. 2 cm in diameter), accessible with a long-reach tree pruner, was collected for each tree (with a maximum height of approx. 20 m). Old leaves (the first four on the branch), young leaves (the last four on the branch) and twigs (at the tip of the branch) were collected in the field, and wood samples were obtained by stripping off the bark from the wood of the branches using a sharp box cutter in the laboratory after being oven-dried. Bark and wood samples were collected from branches. Latex samples of Sapotaceae were collected by cutting a groove 1 cm deep into the trunk and collecting the

Figure 5. Location of the plot and trees in the Plaine de Lac.

(a) Plot in the New Caledonian archipelago.
 (b) Overview false-colour image of the plot surroundings.
 (c) Close-up RGB image of the plot with identified hyperaccumulator trees.
 (d) Close-up RGB image of the plot with all of the trees (diameter at breast height, dbh > 10 cm). Key: grey polygons, plots; green circles, all trees; light-green circles, *Pycnanandra acuminata*; yellow circles, *Homalium guillauminii*; red circles, *Geissois pruinosa* var. *pruinosa*; blue pentagons, litterfall traps. The size of the circles indicates the relative tree diameter.



exudate. The xylem sap was obtained from harvested branches using a handheld vacuum pump after bark removal to avoid contamination with phloem sap or latex (Alexou and Peuke, 2013). Litterfall was collected once a month for 12 months in $12 \times 1 \text{ m}^2$ litterfall traps randomly positioned in the plot. The plant samples were oven-dried for 3 days at 60°C (leaves, twigs and branches) or freeze-dried (xylem sap and latex) by lyophilising in a freeze dryer (-85°C at <0.003 millibar) for 48 hours. All plant samples were ground to a fine powder in an impact mill and weighed into $300 \pm 20 \text{ mg}$ in 50-ml polypropylene tubes. These samples were pre-digested using 7 ml of HNO_3 (70%) for 48 hours before being closed into vessels and digested for 45 min in a microwave oven at 125°C (Milestone Start D). Following digestion, the samples were diluted to 50 ml with ultrapure deionised water ($18.2 \text{ M}\Omega \text{ cm}^{-1}$ at 25°C ; Millipore, now Merck, <https://www.merckmillipore.com>).

Collection and processing of soil samples

One soil sample was collected at four different depths: 0–5, 5–10, 10–15 and 15–20 cm at random locations in each subplot. The soil samples were air-dried for a week and then sieved through 2-mm screens. A $\text{Sr}(\text{NO}_3)_2$ -extraction (0.01 M) was performed using a method adapted from Kukier & Chaney to determine weakly exchangeable Ni concentrations in the soil (solid/liquid ratio, m:v, of 1:4 for 2 h) (Kukier and Chaney, 2001). The potential phytoavailable metal concentrations in soils were determined using

diethylenetriaminepentaacetate (DTPA)-extraction, excluding triethanolamine, with a solid/liquid ratio (m:v) of 1:5 at pH 5.3, after shaking on an end-over-end shaker for 2 h (adapted from Lindsay and Norvell, 1978). Pseudo-total concentrations in soils were determined by weighing approximately 100 mg of soil subsamples into digestion tubes with strong acid extraction using reverse aqua regia (3:1 HNO_3 :HCl) for 16 min at 50% power in a ColdBlock system (CB15S 15 channel system; ColdBlock Technologies Inc., <https://coldblock.ca>) with high-intensity infrared irradiation (Wang *et al.*, 2014). The digests were diluted to 50 ml with ultrapure deionised water (Millipore) and filtered (Whatman® grade-1 filter paper; Whatman, now cytiva, <https://www.cytivalifesciences.com>).

Elemental analysis of plant and soil samples

All acid digests and extracts were analysed by inductively coupled plasma atomic emission spectroscopy (ICP-AES) for trace elements (Co, Mn, Ni and Zn). Radial and axial modes were used depending on the element and expected analyte concentrations. In-line internal addition standardisation using yttrium was used to compensate for any matrix-based interference. Quality controls included matrix blanks, standard reference material (Apple Leaves, NIST 1515; National Institute of Science and Technology, <https://www.nist.gov>) and internal reference materials (powdered *R. cf. bengalensis* for plant samples and sieved ultramafic soil collected at Mont Mou, New Caledonia, for soil samples).



Figure 6. The 0.25-ha Plaine des Lacs plot sampling was conducted from March to May 2018.

- (a) *Pycnanthus acuminatus* trees were identified with red tape during the sampling period.
 (b) Litterfall and soil samples were collected in each subplot (white arrows show *P. acuminatus* leaves).
 (c) Each *P. acuminatus* tree was excised and the blue–green latex was collected.
 (d) The 100 subplots were delimited with blue cords.

Nickel stable isotope analysis in soil and plant samples

All sample handling was conducted in a cleanroom at the Commonwealth Scientific and Industrial Research Organisation (CSIRO) Waite Campus in Adelaide. Perfluoroalkoxy (PFA) vials and multi-collector autosampler tubes were cleaned by fluxing with concentrated HCl for 24 h, then concentrated HNO₃ for 24 h, followed by immersion in ultrapure deionised water (Milli-Q, MQ; Millipore). Single-distilled 70% HNO₃ (Thermo Fisher Scientific, <https://www.thermofisher.com>) was used for sample digestions, resin cleaning and ion-exchange chromatography. Hydrogen peroxide (30% H₂O₂; Rowe Scientific, <https://www.rowe.com.au>) was also used for sample digestion. Single-distilled 37% HCl (Scharlau, <https://www.scharlab.com>) was used for cleaning vials and ion-exchange chromatographic columns. Certified reference materials (CRMs) used for method validation were sourced from NIST (nickel isotopic standard NIST 986 and Montana soil NIST 2711a) and the US Geological Survey (Nod-P-1 manganese nodule). Background levels of Ni were monitored by preparing a procedural

blank, wherein the acid reagents were treated using the same method as the samples. One in four samples was prepared in duplicate to check for the reproducibility of the method.

Approximately 100–200 mg of plant material (old leaves, young leaves, wood and latex from three *P. acuminatus* trees) and soil samples (5, 10, 15 and 20 cm depth, located near *P. acuminatus* trees) were weighed into Teflon microwave pressure vessels. The reproducibility of the method was assessed by the use of duplicates every six samples. A mix of 7.5 ml of concentrated HNO₃ and 2.5 ml of concentrated HCl was added and digested in closed vessels at 170°C for 30 min using a microwave oven set at 1500 W (Anton-Paar, <https://www.anton-paar.com>). The solutions were transferred to clean 50-ml PFA vials, then 1 ml of H₂O₂ was added and the samples were heated overnight at 140°C. The samples were then evaporated and taken up in 5 ml of 0.5 M HCl and centrifuged to remove particulates. Approximately 0.5 ml of solution was analysed for Ni concentrations by ICP-AES (Agilent 5100; Agilent, <https://www.agilent.com>).

For soil samples, an aliquot of digest solution equivalent to 10–15 µg of Ni was taken for the ion-exchange chromatography purification procedure. The separation and purification of Ni, and its chemical considerations, have been described previously (Chernozhukin *et al.*, 2015; Gall, 2011; Gueguen *et al.*, 2013; Wu *et al.*, 2019). Separation of Ca, Fe and Mg from Ni in the samples is necessary as these elements can cause isobaric and polyatomic interference when measuring Ni isotopes (Chernozhukin *et al.*, 2015). The purification procedure is detailed in Method S1 and can be summarised as: (i) the removal of Cu and Fe using AG1-X8 resin; (ii) the separation of Ni from matrix elements using Ni-specific resin; and (iii) the final removal of Fe using AG1-X8 resin. In contrast to the soil samples, plant and natural latex samples contain low ratios of Ca, Mg, Ti and Fe to Ni (Method S2). Therefore, only the second and third steps of the nickel purification procedure were used.

After purification, solutions were evaporated to dryness and the residue was resuspended in 0.2 ml of concentrated HNO₃ to destroy organic residues leached from the resins. This process was repeated until a pale-green residue remained. This residue was then resuspended in 2 ml of 2% HNO₃. Approximately 0.5 ml of the Ni purified solution was analysed by ICP-AES and/or inductively coupled plasma mass spectrometry (ICP-MS) (Agilent 8800 Triple Quadrupole ICP-MS; Agilent) to determine Ni recovery and ensure the absence/elimination of potential interfering ions during MC-ICP-MS analysis (e.g. Cu, Fe, Mn, Mg, Na and Ti). The $\delta^{60}\text{Ni}/^{58}\text{Ni}$ isotopic ratio calculation ($\delta^{60}\text{Ni}$) followed the method described by Gueguen *et al.* (2013) and Guignard *et al.* (2020) (Method S3–S4).

Nickel recovery from Ni-specific resin for soil samples ranged from 90 to 98% (Method S5). The isotopic standard NIST 986 was processed through the Ni purification procedure and the $\delta^{60}\text{Ni}$ ratios were within error for unprocessed samples (Method S6), demonstrating the no isotopic fractionation occurred during the column purification process. Certified reference material 2711a returned a $\delta^{60}\text{Ni}$ isotope ratio of $0.05 \pm 0.1\text{‰}$ and CRM Nod-P-1 returned a $\delta^{60}\text{Ni}$ isotope ratio of $0.49 \pm 0.10\text{‰}$ (Method S6). These results were within the analytical error of previously published results of 0.14 and 0.39‰, respectively (Gall, 2011; Ratié *et al.*, 2015; Wu *et al.*, 2019). However, it should be noted that the digestion procedure used in this study (aqua regia) was a strong acid leach, which is known to be less aggressive in the extraction of metals such as Ni from soils and minerals than with strong acid digestion procedures using hydrofluoric acid (Ratié *et al.*, 2015). The recoveries of Ni from the Montana soil CRM 2711a and Mn Nodule Nod-P-1 in this study were $18.6 \pm 0.40 \mu\text{g g}^{-1}$ (86%

recovery) and $1.29 \pm 0.40 \mu\text{g g}^{-1}$ (92% recovery), respectively. The observed differences between our $\delta^{60}\text{Ni}$ ratios for soil CRMs and those reported in the literature may relate to an inability to extract/remove Ni from residual fractions in soils (e.g. silicates). The concentration of Ni in procedural blank samples after ion-exchange chromatography was between 4 and 25 ng Ni, representing a negligible contribution to the total Ni processed in samples analysed by MC-ICP-MS (10–15 μg).

Nickel isotope ratios (^{58}Ni and ^{60}Ni) were determined using MC-ICP-MS (Neptune; ThermoFisher Scientific, <https://www.thermo.com>) housed at the CSIRO Waite Campus. The samples were measured in 2% HNO_3 at Ni concentrations of about $1 \mu\text{g L}^{-1}$. Faraday detector cups were set up to detect the masses ^{57}Fe , ^{58}Ni , ^{60}Ni , ^{61}Ni , ^{62}Ni , ^{63}Cu and ^{65}Cu in medium resolution mode. Samples were aspirated using a $50 \mu\text{l min}^{-1}$ nebuliser into a quartz spray chamber with a Scott double-pass configuration and X-geometry skimmer cones. The Ni purified solution was spiked with an in-house Cu isotopic standard solution (final concentration $500 \mu\text{g L}^{-1}$ Cu) for external mass bias correction using the exponential law. The isotopic Cu standard NIST 976 is a widely used isotopic standard; however, this standard is no longer available. Instead, an in-house isotopic Cu standard (STD1) with a $^{65}\text{Cu}/^{63}\text{Cu}$ of 0.4455 was used, which is very similar to that of NIST 976 (0.4456) (Ryan *et al.*, 2013). An instrument baseline and peak centre were performed before each sample and bracketing standard. Isotope ratios were measured in one block consisting of 40 cycles with a 4 sec integration time. Each sample was measured a minimum of four times. The ^{57}Fe mass was measured for each sample and signals of the order of 6e^{-3} V were a negligible contribution to the signal intensity.

Statistical analyses

The data generated in this study were analysed using RSTUDIO 1.1.456 (<https://www.rstudio.com>). Medians (minimum–maximum) were determined using the descriptive analysis tool and significant differences were tested using two-way analysis of variance (ANOVA) with a confidence level of 95%. Means were separated by the Duncan–Waller *K* ratio *t*-test, as it is a more conservative test. The homogeneity of variance was tested by Levene's test, and the normality of the residuals was tested by the Shapiro–Wilk test; necessary log transformations were applied. The dbh refers to the tree diameter at 1.3 m above the ground. The HBI of a tree was defined as the sum of the hyperaccumulator tree dbh located in a 15-m radius and was used to assess the influence of this specific group on the local ecosystem. Plant biomass was determined with the seventh model proposed by Chave *et al.* (2014), whereas plant part masses were calculated using ratios determined from the tropical rainforest allometric formula proposed by Yamakura *et al.* (1986). Wood densities were obtained from external organisation databases from the literature (e.g. Brown, 1997; ICRAF, 2013) and from the NC-PIPPN database (Birnbaum *et al.*, 2015). In the absence of a value for a species, wood density was used from the values known for the genus (Chave *et al.*, 2006).

Stocks were calculated by multiplying individual biomasses with plant part concentrations. Elemental maps were made via ARCMAP 10.7.1 (2019-06-27; ESRI, <https://www.esri.com>) using the near-neighbour interpolation. This procedure uses the closest input values to a defined point and applies weights based on proportionate areas to interpolate a value (Sibson, 1981). Each map (Co, Mn, Ni and Zn) was developed based on the ICP-AES values from the same soil cores (one sample per depth and subplot).

ACKNOWLEDGEMENTS

This research was undertaken in collaboration with the Institut de Recherche pour le Développement. We thank Bruno Fogliani, Vanessa Hequet, William Nigote and Anthony Pain for their support during the fieldwork, Thomas Ibanez for help in the transformation of georeferenced data and Philippe Birnbaum for sharing plot data from the NC-PIPPN. AVDE was the recipient of a Discovery Early Career Researcher Award (DE160100429) from the Australian Research Council. ALDP was the recipient of an Australian Government Research Training Program Scholarship at The University of Queensland, Australia.

AUTHOR CONTRIBUTIONS

Research concept and design: ALDP, AVDE, SI and PDE. Sample collection: ALDP and SI. Sample processing: ALDP and CMW. Manuscript writing: ALDP and AVDE. Review & editing: AJMB, GE, PDE, CMW, SI and JKK. All authors participated in discussion of the research.

CONFLICT OF INTEREST

The authors declare that they have no conflicts of interest associated with this work.

DATA AVAILABILITY STATEMENT

All relevant data supporting the findings of this work are available within the article and the supporting material. Additional data not included in the supporting material are available upon request to the corresponding author.

SUPPORTING INFORMATION

Additional Supporting Information may be found in the online version of this article.

Figure S1. Spatial distribution of $\text{Sr}(\text{NO}_3)_2$ -extractable Co concentrations (mg kg^{-1}).

Figure S2. Spatial distribution of DTPA-extractable Co concentrations (mg kg^{-1}).

Figure S3. Spatial distribution of pseudo-total Co concentrations (mg kg^{-1}).

Figure S4. Spatial distribution of $\text{Sr}(\text{NO}_3)_2$ -extractable Mn concentrations (mg kg^{-1}).

Figure S5. Spatial distribution of DTPA-extractable Mn concentrations (mg kg^{-1}).

Figure S6. Spatial distribution of pseudo-total Mn concentrations (mg kg^{-1}).

Figure S7. Spatial distribution of $\text{Sr}(\text{NO}_3)_2$ -extractable Zn concentrations (mg kg^{-1}).

Figure S8. Spatial distribution of DTPA-extractable Zn concentrations (mg kg^{-1}).

Figure S9. Spatial distribution of pseudo-total Zn concentrations (mg kg^{-1}).

Figure S10. Spatial distribution of the ratio of $\text{Sr}(\text{NO}_3)_2$ -extractable Co to pseudo-total Co.

Figure S11. Spatial distribution of the ratio of DTPA-extractable Co to pseudo-total Co.

Figure S12. Spatial distribution of the ratio of $\text{Sr}(\text{NO}_3)_2$ -extractable Mn to pseudo-total Mn.

Figure S13. Spatial distribution of the ratio of DTPA-extractable Mn to pseudo-total Mn.

Figure S14. Spatial distribution of the ratio of $\text{Sr}(\text{NO}_3)_2$ -extractable Ni to pseudo-total Ni.

Figure S15. Spatial distribution of the ratio of DTPA-extractable Ni to pseudo-total Ni.

Figure S16. Spatial distribution of the ratio of $\text{Sr}(\text{NO}_3)_2$ -extractable Zn to pseudo-total Zn.

Figure S17. Spatial distribution of the ratio of DTPA-extractable Zn to pseudo-total Zn.

Table S1. Statistical significance of the HBI index and species.

Table S2. Cobalt concentrations in diverse plant parts of the species in the plot.

Table S3. Zinc concentrations in diverse plant parts of the species in the plot.

Table S4. Mn concentrations in diverse plant parts of the species in the plot.

Table S5. Soil pH of the plot across the soil profile.

Table S6. Total quantities of trace elements returning to the soil via litterfall.

REFERENCES

- Alexander, E. & DuShay, J. (2011) Topographic and soil differences from peridotite to serpentinite. *Geomorphology*, **135**(3–4), 271–276.
- Alexou, M. & Peuke, A.D. (2013) Methods for xylem sap collection. In: Maathuis, F.J. (Ed.) *Plant Mineral Nutrients: Methods and Protocols*. Totowa: Humana Press, pp. 195–207.
- Baker, A.J.M. (2009) A Darwinian approach to mine closure and restoration. In: *Proceedings of the Fourth International Conference on Mine Closure* (Fourie, A.B. & Tibbett, M., eds). Perth: Australian Centre for Geomechanics, pp. 21–23.
- Baker, A.J.M., Ernst, W.H.O., van der Ent, A., Malaisse, F. & Ginocchio, R. (2010) Metallophytes: the unique biological resource, its ecology and conservational status in Europe, central Africa and Latin America. In: *Ecology of Industrial Pollution* (Batty, L.C. & Hallberg, K.B., eds). Cambridge: Cambridge University Press, pp. 7–39.
- Birnbaum, P., Ibanez, T., Pouteau, R., Vandrot, H., Hequet, V., Blanchard, E. et al. (2015) Environmental correlates for tree occurrences, species distribution and richness on a high-elevation tropical island. *AoB Plants*, **7**, p.plv075.
- Boyd, R. (2007) The defense hypothesis of elemental hyperaccumulation: status, challenges and new directions. *Plant and Soil*, **293**(1–2), 153–176.
- Boyd, R. (2012) Plant defense using toxic inorganic ions: Conceptual models of the defensive enhancement and joint effects hypotheses. *Plant Science*, **195**, 88–95.
- Boyd, R.S. & Jaffré, T. (2001) Phytoenrichment of soil Ni content by *Sebertia acuminata* in New Caledonia and the concept of elemental allelopathy. *South African Journal of Science*, **97**, 535–538.
- Boyd, R.S. & Martens, S.N. (1998) The significance of metal hyperaccumulation for biotic interactions. *Chemoecology*, **8**, 1–7.
- Brooks, R.R. (1987) *Serpentine and Its Vegetation: A Multidisciplinary Approach*. Portland: Dioscorides Press.
- Brown, S. (1997) *Estimating Biomass and Biomass Change of Tropical Forests: A Primer*. Urbana: Food & Agriculture Forestry Paper.
- Chave, J., Muller-Landau, H.C., Baker, T.R., Easdale, T.A., Steege, H.T. & Webb, C.O. (2006) Regional and phylogenetic variation of wood density across 2456 neotropical tree species. *Ecological Applications*, **16**(6), 2356–2367.
- Chave, J., Réjou-Méchain, M., Búrquez, A., Chidumayo, E., Colgan, M., Delitti, W. et al. (2014) Improved allometric models to estimate the aboveground biomass of tropical trees. *Global Change Biology*, **20**(10), 3177–3190.
- Chernozhukhin, S., Goderis, S., Lobo, L., Claeys, P. & Vanhaecke, F. (2015) Development of an isolation procedure and MC-ICP-MS measurement protocol for the study of stable isotope ratio variations of nickel. *Journal of Analytical Atomic Spectrometry*, **30**(7), 1518–1530.
- Datta, S., Chaudhury, K. & Mukherjee, P. (2015) Hyperaccumulators from the serpentine of Andaman, India. *Australian Journal of Botany*, **63**(4), 243–251.
- Deng, T.H.B., Cloquet, C., Tang, Y.T., Sterckeman, T., Echevarria, G., Estrade, N. et al. (2014) Nickel and zinc isotope fractionation in hyperaccumulating and nonaccumulating plants. *Environmental Science and Technology*, **48**(20), 11926–11933.
- Deng, T., Tang, Y., van der Ent, A., Sterckeman, T., Echevarria, G., Morel, J.L. et al. (2016) Nickel translocation via the phloem in the hyperaccumulator *Nocca caerulea* (Brassicaceae). *Plant and Soil*, **404**(1–2), 35–45.
- Echevarria, G. (2021) Genesis and behaviour of ultramafic soils and consequences for nickel biogeochemistry. In: *Agromining: Farming for Metals*. 2nd edn (van der Ent, A., Baker, A.J.M., Simonnot, M.-O. & Morel, J.L., eds). Cham: Springer Nature, pp. 215–238.
- Estrade, N., Cloquet, C., Echevarria, G., Sterckeman, T., Deng, T., Tang, Y. et al. (2015) Weathering and vegetation controls on nickel isotope fractionation in surface ultramafic environments (Albania). *Earth and Planetary Science Letters*, **423**, 24–35.
- Galey, M.L., van der Ent, A., Iqbal, M.C.M. & Rajakaruna, N. (2017) Ultramafic geocology of South and Southeast Asia. *Botanical Studies*, **58**(1), 18.
- Gall, L. (2011) *Development and Application of Nickel Stable Isotopes as a New Geochemical Tracer*. Oxford: University of Oxford.
- Gei, V., Isnard, S., Erskine, P.D., Echevarria, G., Fogliani, B., Jaffré, T. et al. (2020) A systematic assessment of the occurrence of trace element hyperaccumulation in the flora of New Caledonia. *Botanical Journal of the Linnean Society*, **194**(1), 1–22.
- Ghaderian, S.M., Ghasemi, R. & Hajhashemi, F. (2015) Interaction of nickel and manganese in uptake, translocation and accumulation by the nickel-hyperaccumulator plant, *Alyssum bracteatum* (Brassicaceae). *Australian Journal of Botany*, **63**(2), 47.
- Grandcolas, P., Murienne, J., Robillard, T., Desutter-Grandcolas, L., Jourdan, H., Guilbert, E. et al. (2008) New Caledonia: a very old Darwinian island? *Philosophical Transactions of the Royal Society of London. Series B, Biological Sciences*, **363**(1508), 3309–3317.
- Gueguen, B., Rouxel, O., Ponzevera, E., Bekker, A. & Fouquet, Y. (2013) Nickel isotope Variations in terrestrial silicate rocks and geological reference materials measured by MC-ICP-MS. *Geostandards and Geoanalytical Research*, **37**(3), 297–317.
- Guignard, J., Quitté, G., Méheut, M., Toplis, M.J., Poitrasson, F., Connetable, D. & Roskosz, M. (2020) Nickel isotope fractionation during metal-silicate differentiation of planetesimals: Experimental petrology and ab initio calculations. *Geochimica et Cosmochimica Acta*, **269**, 238–256.
- Ibanez, T., Munzinger, J., Dagostini, G., Hequet, V., Rigault, F., Jaffré, T. et al. (2013) Structural and floristic diversity of mixed tropical rain forest in New Caledonia: new data from the New Caledonian Plant Inventory and Permanent Plot Network (NC-PIPPN). *Applied Vegetation Science*, **17**(3), 386–397.
- ICRAF. (2013). *Worldwide "Open Access" The functional attributes and ecological database*. [online] Available at: <http://db.worldagroforestry.org/>. Accessed March 1, 2021.
- Isnard, S., L'Huillier, L., Paul, A.L.D., Munzinger, J., Fogliani, B., Echevarria, G. et al. (2020) Novel insights into the hyperaccumulation syndrome in *Pycnanthus* (Sapotaceae). *Frontiers in Plant Science*, **11**, 559059.
- Isnard, S., L'Huillier, L., Rigault, F. & Jaffré, T. (2016) How did the ultramafic soils shape the flora of the New Caledonian hotspot? *Plant and Soil*, **403**(1–2), 53–76.
- Jaffré, T. (1980) *Étude écologique du peuplement végétal des sols dérivés de roches ultrabasiques en Nouvelle Calédonie*. Paris: Travaux et Documents de l'ORSTOM.
- Jaffré, T. (1993) The Relationship between ecological diversity and floristic diversity in New Caledonia. *Biodiversity Letters*, **1**(3–4), 82–87.
- Jaffré, T., Brooks, R.R., Lee, J. & Reeves, R.D. (1976) *Sebertia acuminata*: A hyperaccumulator of nickel from New Caledonia. *Science*, **193**(4253), 579–580.
- Jaffré, T. & L'Huillier, L. (2010) La végétation des roches ultramafiques ou terrains miniers. In: *Mines et Environnement en Nouvelle-Calédonie: les milieux sur substrats ultramafiques et leur restauration* (L'Huillier, L., Jaffré, T. & Wulff, A. eds). Nouméa: IAC Édition, pp. 45–103.

- Jaffré, T., Reeves, R.D., Baker, A.J.M., Schat, H. & van der Ent, A. (2018) The discovery of nickel hyperaccumulation in the New Caledonian tree *Pycnanandra acuminata* 40 years on: an introduction to a Virtual Issue. *New Phytologist*, **218**(2), 397–400.
- Kerfoot, O. (1963) The root systems of tropical forest trees. *The Commonwealth Forestry Review*, **42**, 19–26.
- Kukier, U. & Chaney, R.L. (2001) Amelioration of nickel phytotoxicity in muck and mineral soils. *Journal of Environmental Quality*, **30**(6), 1949–1960.
- Latham, M., Quantin, P. & Aubert, G. (1978) *Étude des Sols de la Nouvelle-Calédonie*. Nouméa: ORSTOM.
- Lindsay, W.L. & Norvell, W.A. (1978) Development of a DTPA soil test for zinc, iron, manganese, and copper. *Soil Science Society of America Journal*, **42**(3), 421–428.
- Lopez, S., Benizri, E., Erskine, P.D., Cazes, Y., Morel, J.L., Lee, G. *et al.* (2019) Biogeochemistry of the flora of Weda Bay, Halmahera Island (Indonesia) focusing on nickel hyperaccumulation. *Journal of Geochemical Exploration*, **202**, 113–127.
- McCoy, S., Jaffré, T., Rigault, F. & Ash, J.E. (1999) Fire and succession in the ultramafic maquis of New Caledonia. *Journal of Biogeography*, **26**(3), 579–594.
- Mesjasz-Przybyłowicz, J., Przybyłowicz, W., Barnabas, A. & van der Ent, A. (2016) Extreme nickel hyperaccumulation in the vascular tracts of the tree *Phyllanthus balgooyi* from Borneo. *New Phytologist*, **209**(4), 1513–1526.
- Météo France (2021). *Données Publiques de Météo-France—Accueil*. [online]. Available at: <https://donneespubliques.meteofrance.fr/>. Accessed March 1, 2021.
- Morat, P., Jaffré, T., Tronchet, F., Munzinger, J., Pillon, Y., Veillon, J.-M. *et al.* (2012) Le référentiel taxonomique Florical et les caractéristiques de la flore vasculaire indigène de la Nouvelle-Calédonie. *Adansonia*, **34**(2), 179–221.
- Munzinger, J., Morat, P., Jaffré, T., Gâteblé, G., Pillon, Y. & Rouhan, G. *et al.* (2021). FLORICAL: checklist of the vascular indigenous flora of New Caledonia. [online] Available at: <http://publish.plantnet-project.org/project/florical>. Accessed March 1, 2021.
- Navarrete Gutiérrez, D.M., Pollard, A.J., van der Ent, A., Cathelineau, M., Pons, M.N., Cuevas Sánchez, J.A. & Echevarria, G. (2021) *Blepharidium guatemalense*, an obligate nickel hyperaccumulator plant from non-ultramafic soils in Mexico. *Chemoecology*, **31**(3), 169–187.
- Nkrumah, P.N., Baker, A.J.M., Chaney, R.L., Erskine, P.D., Echevarria, G., Morel, J.L. *et al.* (2016) Current status and challenges in developing nickel phytomining: an agronomic perspective. *Plant and Soil*, **406**(1–2), 55–69.
- Paul, A.L.D., Gei, V., Isnard, S., Fogliani, B., Echevarria, G., Erskine, P.D. *et al.* (2020) Nickel hyperaccumulation in New Caledonian *Hybanthus* (Violaceae) and occurrence of nickel-rich phloem in *Hybanthus austrocaledonicus*. *Annals of Botany*, **126**(5), 905–914.
- Pillon, Y., Jaffré, T., Birnbaum, P., Bruy, D., Cluzel, D., Ducousso, M. *et al.* (2020). Infertile landscapes on an old oceanic island: the biodiversity hotspot of New Caledonia. *Biological Journal of the Linnean Society*, **133**, 317–341.
- Pillon, Y., Munzinger, J., Amir, H. & Lebrun, M. (2010) Ultramafic soils and species sorting in the flora of New Caledonia. *Journal of Ecology*, **98**(5), 1108–1116.
- Rascio, N. & Navari-Izzo, F. (2011) Heavy metal hyperaccumulating plants: how and why do they do it? And what makes them so interesting? *Plant Science*, **180**(2), 169–181.
- Ratié, G., Jouvin, D., Garnier, J., Rouxel, O., Miska, S., Guimarães, E. *et al.* (2015) Nickel isotope fractionation during tropical weathering of ultramafic rocks. *Chemical Geology*, **402**, 68–76.
- Ratié, G., Quantin, C., Maia De Freitas, A., Echevarria, G., Ponzevera, E. & Garnier, J. (2019) The behavior of nickel isotopes at the biogeochemical interface between ultramafic soils and Ni accumulator species. *Journal of Geochemical Exploration*, **196**, 182–191.
- Reeves, R.D. (1992) Hyperaccumulation of nickel by serpentine plants. In: *The Vegetation of Ultramafic (Serpentine) Soils* (Baker, A.J.M., Proctor, J. & Reeves, R.D., eds.). Andover, UK: Intercept Ltd, pp. 253–277.
- Reeves, R.D. (2003) Tropical hyperaccumulators of metals and their potential for phytoextraction. *Plant and Soil*, **249**(1), 57–65.
- Reeves, R.D., Baker, A.J.M., Becquer, T., Echevarria, G. & Miranda, Z.J.G. (2007) The flora and biogeochemistry of the ultramafic soils of Goiás state, Brazil. *Plant Soil*, **293**(1–2), 107–119.
- Reeves, R.D., Baker, A.J.M., Borhidi, A. & Berazaín, R. (1999) Nickel hyperaccumulation in the serpentine flora of Cuba. *Annals of Botany*, **83**(1), 29–38.
- Reeves, R.D., van der Ent, A., Echevarria, G., Isnard, S. & Baker, A.J.M. (2021) Global distribution and ecology of hyperaccumulator plants. In: *Agromining: Farming for Metals*, 2nd edn (van der Ent, A., Baker, A.J.M., Simonnot, M.-O. & Morel, J.L., eds.). Cham: Springer Nature, pp. 133–154.
- Ryan, B.M., Kirby, J.K., Degryse, F., Harris, H., McLaughlin, M.J. & Scheiderich, K. (2013) Copper speciation and isotopic fractionation in plants: uptake and translocation mechanisms. *New Phytologist*, **199**(2), 367–378.
- Schlegel, H.G., Cosson, J.-P. & Baker, A.J.M. (1991) Nickel-hyperaccumulating plants provide a niche for nickel-resistant bacteria. *Botanica Acta*, **104**(1), 18–25.
- Sibson, R. (1981) A brief description of natural neighbor interpolation. In: *Interpolating Multivariate Data* (Barnett, V., ed.). New York: John Wiley & Sons, pp. 21–36.
- Tercinier, G. (1963) *Les sols de la Nouvelle-Calédonie*. Nouméa: ORSTOM.
- van der Ent, A., Baker, A.J.M., Reeves, R.D., Pollard, A.J. & Schat, H. (2012) Hyperaccumulators of metal and metalloid trace elements: facts and fiction. *Plant and Soil*, **362**(1–2), 319–334.
- van der Ent, A., Erskine, P. & Sumail, S. (2015) Ecology of nickel hyperaccumulator plants from ultramafic soils in Sabah (Malaysia). *Chemoecology*, **25**(5), 243–259.
- Vitousek, P.M. & Sanford, R.L. (1986) Nutrient cycling in moist tropical forest. *Annual Review of Ecology and Systematics*, **17**(1), 137–167.
- Wang, Y., Kanipayor, R. & Brindle, I.D. (2014) Rapid high-performance sample digestion for ICP determination by ColdBlock™ digestion: part 1 environmental samples. *Journal of Analytical Atomic Spectrometry*, **29**(1), 162–168.
- Wu, G., Zhu, J.M., Wang, X., Han, G., Tan, D. & Wang, S.-J. (2019) A novel purification method for high precision measurement of Ni isotopes by double spike MC-ICP-MS. *Journal of Analytical Atomic Spectrometry*, **34**(8), 1639–1651.
- Yamakura, T., Hagihara, A., Sukardjo, S. & Ogawa, H. (1986) Aboveground biomass of tropical rain forest stands in Indonesian Borneo. *Vegetatio*, **68**, 71–82.
- Zelano, I.O., Cloquet, C., van der Ent, A., Echevarria, G., Gley, R., Landrot, G. *et al.* (2020) Coupling nickel chemical speciation and isotope ratios to decipher nickel dynamics in the *Rinorea cf. bengalensis*-soil system in Malaysian Borneo. *Plant and Soil*, **454**(1–2), 225–243.
- Zelano, I.O., Cloquet, C., Fraysse, F., Dong, S., Janot, N., Echevarria, G. & Montargès-Pelletier, E. (2018) The influence of organic complexation on Ni isotopic fractionation and Ni recycling in the upper soil layers. *Chemical Geology*, **483**, 47–55.